Stability Experiments in the Flow over a Rotating Disk

Stephen P. Wilkinson*
NASA Langley Research Center, Hampton, Virginia
and
Mujeeb R. Malik†
High Technology Corporation, Hampton, Virginia

An experimental study of the transitional flow over a flat disk rotating in quiescent ambient air has been conducted. Using digitized hot-wire data, the axes of the stationary spiral vortices, which are the primary instability mechanisms for the disk flow, have been mapped out in terms of both spatial coordinates and velocity fluctuations. Data are presented for a clean disk and a disk with a single, isolated roughness element. The data show that the spiral vortices are generated at discrete roughness disturbance sites on the disk and that they propagate and grow as wave packets. The familiar vortex pattern of 30 or so vortices results only when these wave packets have merged and filled the entire circumference. The appearance of stationary, secondary instabilities prior to turbulent breakdown has also been observed.

Nomenclature

f = frequency
n = number of vortices
r = local radius
r_D = disk radius
R = Reynolds number, $= r\sqrt{\omega/\nu}$
R_c = Reynolds number at which the spiral vortices begin to amplify
R_T = Reynolds number based on location of transition to turbulence
t = time
u = instantaneous circumferential-velocity fluctuation
$\hat{u}$ = ensemble-averaged circumferential-velocity fluctuation
U = mean circumferential velocity
U_D = local disk velocity
z = height measured normal to disk surface
ζ = nondimensional axial coordinate, $= z\sqrt{\omega/\nu}$
θ = in-plane angular coordinate on disk
λ = wavelength
ν = kinematic viscosity
σ = spatial growth rate
ψ = vortex orientation angle
ω = disk rotational speed

Introduction

THE stability characteristics of three-dimensional boundary layers are of fundamental importance in fluid mechanics. It is widely believed that the instabilities in a boundary layer are triggered by the internalization of environmental disturbances (e.g., freestream turbulence, acoustic waves, surface roughness, vibration, etc.). Once internalized, the instability waves evolve in accordance with linear stability theory until the amplitudes are sufficiently large for nonlinear effects to become dominant. The final breakdown of these nonlinear waves to turbulence occurs very rapidly and is highly three-dimensional even in a simple two-dimensional flow. Although the actual mechanism involved in the internalization is not well understood at this time, the disturbance growth region governed by linear stability theory covers a sufficient portion of the transition process so that very useful information about transition can be obtained from such a theory. Bypasses to this rather simplistic description of the transition phenomenon, however, do commonly occur.[1]

Evolution of two-dimensional linear disturbances in a two-dimensional boundary layer has been studied extensively and is relatively well understood. Problems arise, however, when the flow is three-dimensional, because additional unknowns, e.g., the direction of the disturbance propagation, become important. Furthermore, satisfactory criteria for selecting the disturbances (or packets of disturbances) most responsible for transition have not yet been established for these three-dimensional flows. While considerable success has been achieved in predicting (or more correctly, correlating) transition in three-dimensional boundary layers by using ad hoc theories,[2] definitive experiments are needed to understand the physics of transition in three-dimensional flows.

One fully three-dimensional flow useful in studying transition phenomena is that over a rotating disk in a quiescent ambient fluid. An exact numerical (mean laminar flow) solution to the Navier-Stokes equations for this flow exists which makes it particularly attractive for theoretical stability analysis. Also, the boundary-layer instability mechanism in the flow over the rotating disk is similar to that exhibited in the leading-edge region of a sweptback wing. Both have inflectional cross-flow velocity profiles resulting in the so-called "cross-flow" instability.

Boundary-layer transition on a rotating disk was first studied by Smith[3] using hot-wire techniques. He observed that sinusoidal disturbances appear in the disk boundary layer at sufficiently large Reynolds numbers. Approximately 32 oscillations were observed within one revolution of the disk. Analysis of these data indicated that the disturbances propagate at an angle of approximately 14 deg (measured between a normal to the vortex axis and the radius). Later, in a flow-visualization study using the china-clay technique, Gregory et al.[4] observed 28-31 vortices spiraling outward over the disk at an angle of about 14 deg. The vortices, which appeared stationary relative to the disk, were first observed at a Reynolds number of $R \approx 430$. Transition to turbulence occurred at $R_T \approx 530$. The stationary-vortex flow established in the rotating disk flow was subsequently studied by various investigators.[5-10] These experiments more or less confirmed the observations made by Gregory et al.[4] An additional phenomenon, however, was observed by Fedorov et al.[7] operating at generally higher rotational speeds and using visual (nap-

Presented as Paper 83-1760 at the AIAA 16th Fluid and Plasma Dynamics Conference, July 12-14, 1983; received Feb. 17, 1984; revision received May 9, 1984. This paper is declared a work of the U.S. Government and therefore is in the public domain.

*Aerospace Engineer, Viscous Flow Branch, High-Speed Aerodynamics Division. Member AIAA.
†President. Member AIAA.

thalene) and acoustic techniques. In addition to the 30 or so vortices observed by others, they also noted a region as low as $R=245$ containing 14-16 vortices propagating at an angle of about 20 deg.

Secondary-vortex formation has also been documented. Clarkson et al.,[9] using injected dye and high-speed photography with a disk rotating in water, observed secondary vortices occurring between the primary (inflectional instability) vortices which ultimately led to breakdown to turbulence. This has also been observed by Kobayashi et al.[8] in air using titanium tetrachloride flow visualization.

Among the more notable recent experiments on rotating disk flow is the work of Kitamura.[6] Using hot-wire techniques, he measured the circumferential-velocity fluctuations produced by the vortices. The rms velocity fluctuations, when plotted semilogarithmically, showed a linear region for Reynolds numbers from 430 to 490 associated with the exponential amplification of disturbances in the radial direction.

In other recent experiments, Kobayashi et al.[8] and Malik et al.,[10] both using hot-wire techniques, estimated the critical Reynolds numbers to be 297 and 294, respectively, which tends to confirm the theoretical prediction of 287 by Malik et al.[10] The discrepancy between the values of R_c obtained from hot-wire studies and the earlier relatively high values ($R_c \simeq 400$) obtained by visual techniques clearly results from the insensitivity of the visual techniques to very small disturbances.

In the experiments reported by Malik et al.,[10] the circumferential-velocity fluctuations were measured to Reynolds numbers as low as $R=125$ to test the validity of the linear stability theory calculations also presented in that paper. It was shown that the experimental data supported the theoretical predictions when the effects of Coriolis forces and streamline curvature were included in the theory. Limitations posed by noise levels and the signal-processing techniques available at the time, however, prevented reliable data from being obtained below $R \simeq 294$.

Further definitive experimental data, which are of particular importance to future theoretical work, are still required. Areas of particular concern include: determination of the physics governing the origin of the primary vortices, additional growth rate data for the vortices, the transition Reynolds number, and criteria for the formation of secondary instabilities leading to turbulent breakdown. The current experiment was designed with these areas in mind. An experimental apparatus was constructed to provide a high signal-to-noise ratio for hot-wire measurements at low Reynolds numbers. With this apparatus, the flowfield on a smooth, clean disk has been mapped out in detail using hot-wire and digital signal-processing techniques. The effect of a single, isolated roughness element on the disk flowfield has also been studied using the same techniques.

Experimental Equipment and Apparatus

Rotating-Disk Apparatus

Measurements were conducted with the rotating-disk apparatus shown in Figs. 1 and 2. The overall installation is shown in Fig. 1 and the details of the disk drive system are shown in Fig. 2. The disk itself was an optical-quality glass (schlieren) window chosen for its exceptional flatness (1.25×10^{-4} mm maximum deviation from ideal plane). The air-bearing drive system was used to eliminate mechanical vibration of the apparatus. A flow-control panel with a circular hole exposing the disk surface was used to duct the boundary layer leaving the disk away from the apparatus to avoid interactions with the incoming axial flow. A two-axis traverse mechanism was mounted on a rail supported at the box enclosure wall approximately 200 boundary-layer thicknesses above the disk. Further discussion of the equipment is contained in Ref. 11.

Hot-Wire Measurement System

A single, linearized hot wire was used to measure disturbances in the disk boundary layer. The wire element was approximately 1 mm long with a length-to-diameter ratio of 286. It was positioned parallel to the disk surface and aligned in the radial direction to measure the circumferential-velocity component. The hot wire was calibrated with ambient air in the inlet, potential core region of a duct flow facility located in the same room as the disk facility. The hot-wire signal was high-pass filtered at 0.1 Hz, amplified and input into a 12 bit A/D converter for conversion to 4096 point digital time records at a sample rate of 50,000 samples/s. The overall accuracy for ac measurements including hot-wire calibration was better than ±3%. The A/D converter was triggered by a timing pulse from the rotating disk which insured that the beginning of each time record represented the same angular position on the disk. The digitized data were stored on magnetic tape for later processing.

Experimental Procedure

The experiments consisted of operating the disk at a fixed rotational speed, adjusted such that transition occurred approximately 12 mm from the outer edge, and conducting radial boundary-layer surveys. Fifty equally spaced time records of the u fluctuation were acquired at each radial location at 1.6-s intervals. Each record contained data for approximately 1.2 revolutions of the disk. The hot-wire mean voltage, radial and axial probe position, ambient temperature, and disk rotational speed were also measured and stored for each measurement location.

Two configurations of the disk were tested. For the first test, the disk was cleaned with acetone and wiped with a clean cloth while the disk turned slowly to remove as much at-

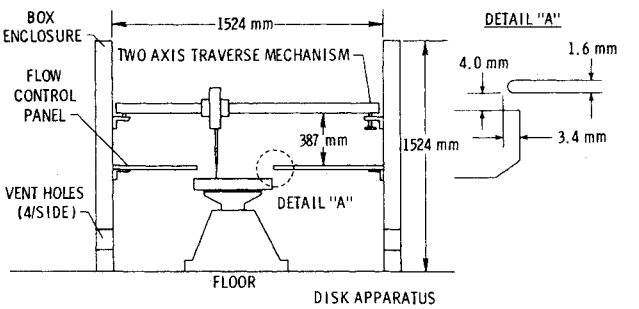

Fig. 1 Rotating-disk apparatus with box enclosure.

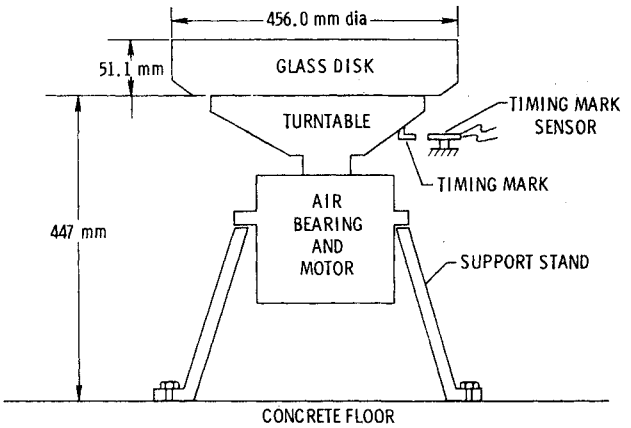

Fig. 2 Rotating-disk drive system.

mospheric dust as possible. This is referred to as the clean disk. A radial boundary-layer traverse at $z = 0.7$ mm ($\zeta = 1.77$) was conducted for this configuration. The second configuration consisted of a single isolated roughness element mounted on an otherwise clean disk. The element was 0.13 mm high by 0.64 mm square and was located at $r = 100$ mm, $\theta = 173$ deg. For this configuration, a radial survey at $z = 0.75$ mm ($\zeta = 1.87$) was conducted. The axial (z) position for the surveys was selected such that the secondary instabilities observed just prior to turbulent breakdown appeared on the oscilloscope at roughly the midpoint of the primary vortices. This is slightly above the peak u intensity height for the primary instability of $\zeta = 1.3$ as suggested in Ref. 6. Since the instabilities measured in this experiment are stationary vortices, a single z location is adequate to characterize the vortex patterns.

Results and Discussion

Clean-Disk Fluctuation Measurements

The first step in analyzing the fluctuation data was to prepare a phase plot of all data for a given run. The phase plot for the clean-disk data is shown in Fig. 3. The abscissa is the disk-rotation angle θ which was derived from original digitized time records as $\theta = \omega t$. The actual data are in the range $0 < \theta < 2\pi$. These data are repeated in the range $2\pi < \theta < 4\pi$ as an aid in visualizing the flowfield. The ordinate for each waveform is the peak-normalized, ensemble-averaged u fluctuation. The vertical placement of each waveform is proportional to its nondimensional radius, r/r_D. A value of $r_D = 229$ mm was used to normalize the radii. The ensemble-averaged waveform consists of the arithmetic mean of all points at each angle θ. Fifty time records were included in each ensemble average. Since all time records began at the same angle, θ, the ensemble-averaging technique substantially reduces the amplitude of all signals which are not stationary with respect to the disk. This includes possible flow oscillations as well as electronic noise. (No attempt was made to search for nonzero phase-velocity disturbance modes.) This technique greatly enhanced the signal-to-noise ratio for the low-intensity (low-R) region.

The next step in analyzing the hot-wire data was to extract the zero-phase velocity disturbance information, i.e., the coordinates of the axes of the primary spiral vortices, from the phase plot (Fig. 3). Guided by the flow-visualization results of Ref. 4, θ for successive peaks from waveform to waveform were cross-plotted with respect to r/r_D. The result is shown in Fig. 4. Each curve in Fig. 4 represents the axis of one of the spiral vortices which are known to be the primary instability mode. Each vortex is labeled with a reference number. There was obvious difficulty in following each vortex to its origin. Large waveform plots and plots of expanded waveforms (i.e., plots of the square root of the peak-normalized data) were helpful in extending the axes to the lower radii, however, most of the features of the flowfields are evident in Fig. 3.

To obtain the familiar spiral vortex pattern provided by flow visualization, the vortex axis data can be plotted in cylindrical coordinates as shown in Fig. 5. A flow-visualization photograph, obtained using the china-clay method and presented in Ref. 4, shows evidence of vortices to Reynolds numbers as low as $R = 430$. The current method shows stationary disturbances to a Reynolds number as low as $R = 150$ (vortex numbers 32 and 33 in Fig. 4).

Referring back to Fig. 3, it is apparent that the primary vortex pattern observed at the outer radii originates at several randomly placed disturbance sites which are presumably small, atmospheric-dust motes which attach to the surface after the disk has been cleaned and generate a stationary disturbance with respect to the disk. Repeat runs, with disk cleaning between each run, indicated the same general behavior but different vortex initiation sites. From linear stability theory it is known that a stationary disturbance

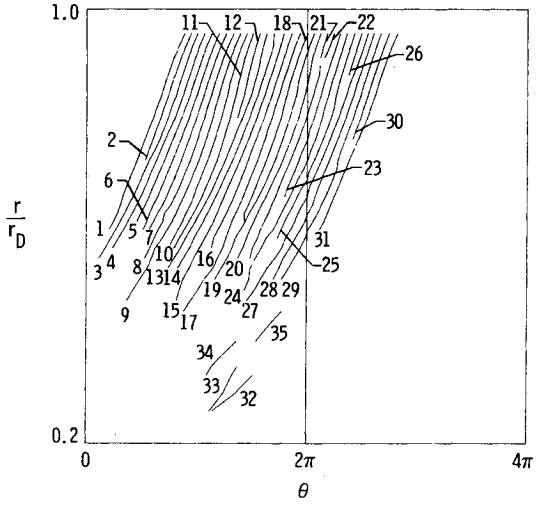

Fig. 4 Cross plot of stationary-vortex axes from phase plot data for clean disk.

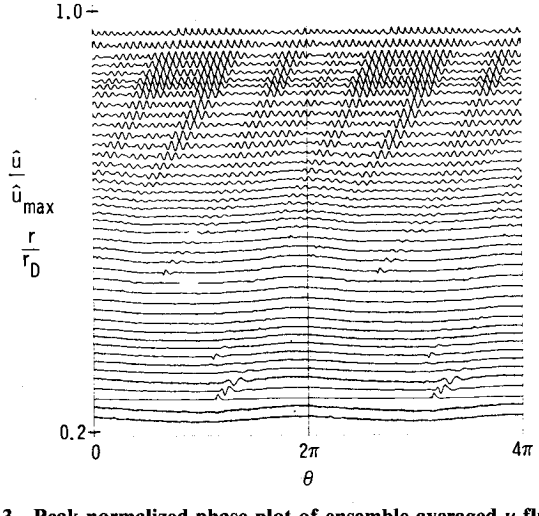

Fig. 3 Peak-normalized phase plot of ensemble-averaged u fluctuation on the clean disk. $\sqrt{\omega/\nu} = 2532$/m, $\zeta = 1.77$, $\omega = 97.83$/s, $r_D = 229$ mm.

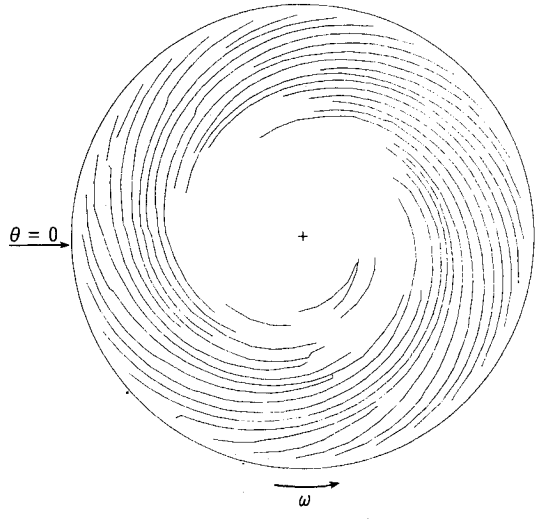

Fig. 5 Stationary-vortex axes in cylindrical coordinates for clean disk.

creates the most unstable frequency.[10] Disturbances from the dust motes propagate and grow as wave packets which intersect at larger radii. Four or, perhaps, five packets can be discerned in Fig. 3. The modulation of the oscillations seen in Fig. 3 and also observed by others[3,6,8] is obviously a result of the wave-packet development. As shown in Fig. 6, the wave-packet spreading phenomena generate an increasing number of vortices, n, as R increases. Up to $R \simeq 250$, only a few decaying vortices are noted. For R in the region of $250 < R < 350$, the wave-packet spreading results in a rapid increase in n. At $R \simeq 350$, the vortices fill the available circumference of the disk and the subsequent rate of increase in n is much slower. The region $R > 350$ contains the familiar 30 or so vortices which have been recorded with flow-visualization techniques in previous studies.[4]

It is seen in Fig. 3 that the angular separation between peaks in the disturbance field (i.e., primarily vortices) varies by only a small amount. The average angular separation, $\Delta\theta$, is approximately 14.2 deg at $r/r_D = 0.5$ and 11.6 deg at $r/r_D = 0.95$ with the decrease resulting from the increase in n, as noted in Fig. 6. (The component of wavelength in the circumferential direction may be obtained from the relation, $\lambda_\theta = r\Delta\theta$.)

The orientation angle, ψ, of the vortices is defined by the relation

$$\tan\psi = \frac{l}{r}\frac{\mathrm{d}r}{\mathrm{d}\theta} \tag{1}$$

Using second-order, least-square curve fits to each of the vortex axes in Fig. 4, it was determined that the angle ψ was predominantly in the range of 11-14 deg. The theoretical prediction[10] is about 11.2 deg. (The radial component of wavelength is defined as $\lambda_r = \lambda_\theta \sin\psi$.)

The amplitude growth for each vortex in Fig. 4 is shown in Fig. 7. The ordinate for each plot is the natural logarithm of the ensemble-averaged u fluctuation. The low-frequency oscillation, which was produced by very small disk misalignment and was evident at the lower radii in Fig. 3 for $f = \omega$, was digitally filtered out before plotting the growth data. The data are based on the positive peak amplitude in $\hat{u}$. A variety of general features of the flowfield are indicated in Fig. 7. The most evident feature is that all of the vortices nominally exhibit an exponential growth region (linear variation on log plot). The low Reynolds number region is generally characterized by large scatter in the data (e.g., vortex numbers 9 and 24). Certain vortices show an exponential growth rate which levels off at an intermediate Reynolds number and then enters a new exponential growth region. The phenomenon is seen clearly, for example, in vortices 4, 13, and 31. This behavior can be traced back to the regions where adjacent wave packets intersect in Fig. 3. Another notable feature of the data is the leveling off in growth as turbulent breakdown is approached (e.g., vortices 29 and 30). A final general note is that at low Reynolds numbers certain vortices apparently decay and disappear, as in vortices 32-35, or decay until a critical Reynolds number is attained and thereafter grow, as in vortices 13 and 17. No vortex growth is observed at a Reynolds number below about $R = 300$ indicating that the theoretical value for the minimum critical Reynolds number of $R = 287$ is reasonable.[10]

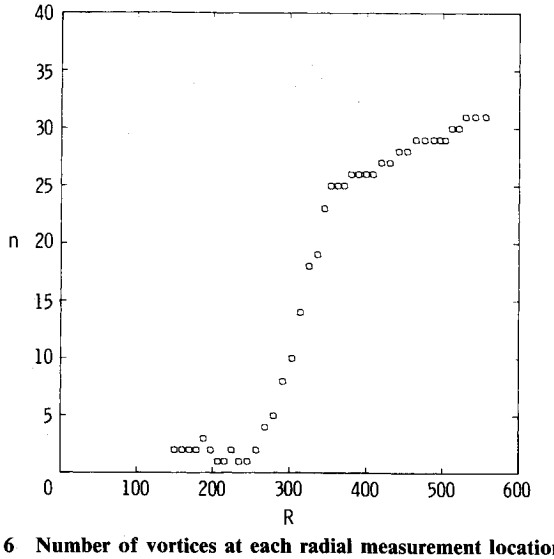

Fig. 6 Number of vortices at each radial measurement location on clean disk.

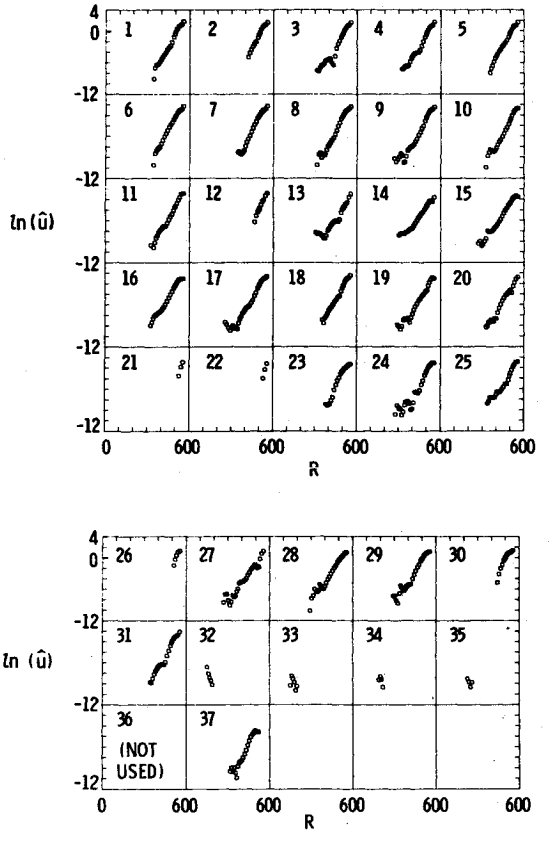

Fig. 7 Peak ensemble-averaged fluctuation velocity for each clean-disk vortex (u in m/s).

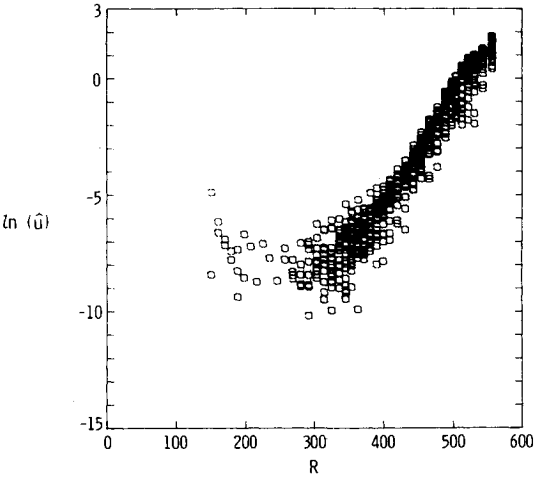

Fig. 8 Overlay of all growth data for clean disk (u in m/s).

To illustrate the variation in $\hat{u}$ with both R and θ more concisely, an overlay of all of the individual plots in Fig. 7 is shown in Fig. 8. The variance in $\hat{u}$ at constant R is caused by the nonuniform growth of the four or five packets evident in Fig. 3. Figure 9 shows the circumferential variation in $\hat{u}$ at several values of R.

The growth rate for the fluctuation data is defined as

$$\sigma = \frac{d[\ell n(u/u_0)]}{dR} \tag{2}$$

where $\hat{u}_0$ is the disturbance amplitude at the beginning of the vortex. (Since $\hat{u}_0$ is, by definition, a constant, its value is not required to be known in order to calculate σ.) A cursory evaluation of Fig. 7 shows that the experimental values of σ vary considerably over the Reynolds number range for each of the vortex growth curves shown. Furthermore, this variation is also a function of θ. Figure 10 shows the growth-rate variation with θ at $R=489$ in the exponential growth-rate region of the flowfield. The data were obtained by least-square fitting a straight-line segment to five successive points in each plot of Fig. 7 centered on $R=489$. The theoretical value of σ from Ref. 10 at $R=489$ is $\sigma=0.073$. Figure 10 shows that the

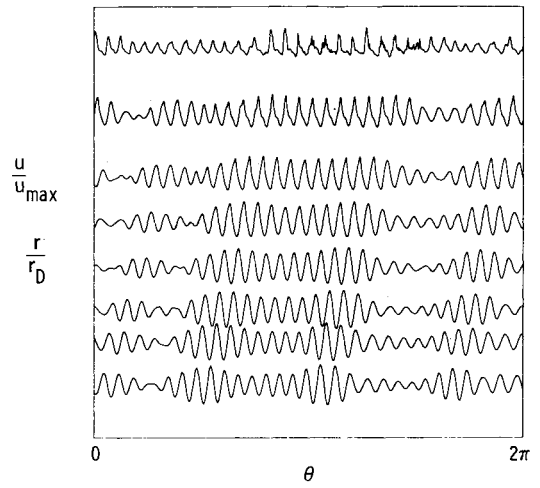

Fig. 11 Phase plot of instantaneous u in region of turbulent breakdown on clean disk. (From bottom to top: $r/r_D=0.839$, 0.853, 0.865, 0.978, 0.895, 0.911, 0.932, 0.955.)

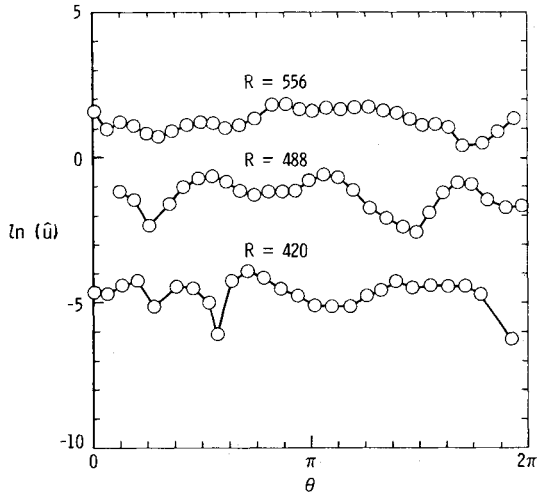

Fig. 9 Peak ensemble-averaged fluctuation velocity at three Reynolds numbers on clean disk (u in m/s).

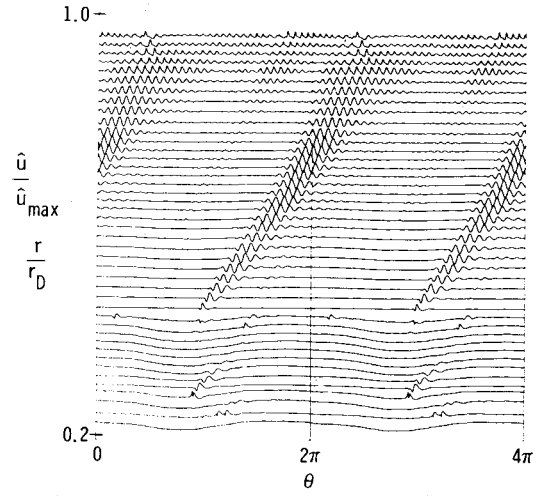

Fig. 12 Peak-normalized phase plot of ensemble-averaged u fluctuation on disk with roughness element. $\sqrt{\omega/\nu}=2491$/m, $\zeta=1.87$, $\omega=95.63$/s, $r_D=229$ mm.

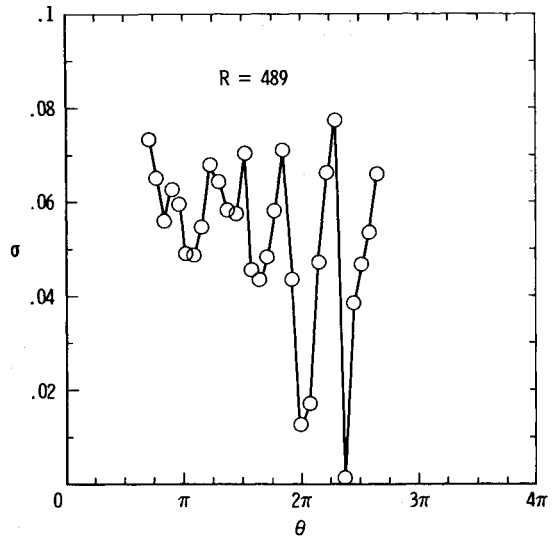

Fig. 10 Spatial growth rate of stationary vortices at $R=489$ on clean disk.

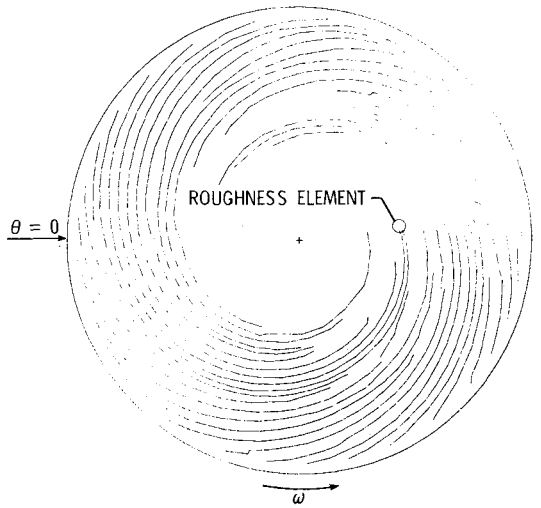

Fig. 13 Stationary-vortex axes in cylindrical coordinates for disk with roughness element.

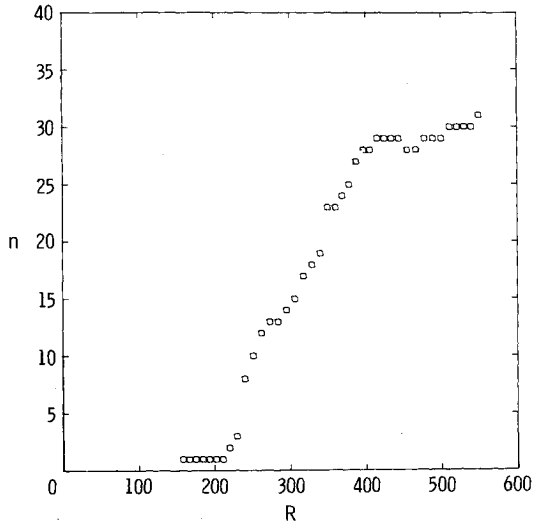

Fig. 14 Number of vortices at each radial measurement location on disk with roughness element.

growth rate measured through a wave packet at constant R depends not only on R, but also on the state of development of the wave packet. As indicated previously, the vortex pattern at $R=489$ results from four or five intersecting wave packets. This roughly corresponds to the number of oscillations in σ shown in Fig. 10 for one revolution of the disk.

A final topic of consideration for the clean disk is the actual breakdown to turbulence. Figure 11 shows a phase plot of the instantaneous, peak-normalized u fluctuation for the outer eight radial measurement locations. The top trace shows local turbulent breakdown in the range $\pi<\theta<3\pi/2$. No turbulent breakdown was observed in the previous trace which places the transition Reynolds number in the range $543<R_T<556$. Turbulent breakdown was always preceded by stationary, secondary instabilities. These are seen in the central region of the next-to-the-top trace in Fig. 11 as inflections of the primary vortices. These secondary instabilities are presumably free-shear-layer-type instabilities due to the intense vertical shear region between adjacent, like-rotating primary vortices. Also apparent in Fig. 11 is the spectral broadening of the waveform as turbulence is approached. The bottom-most waveform is nearly sinusoidal and progresses to approximately a triangular signal in the next-to-the-top trace. The occurrence of the secondary instabilities is the final stage of the transition process.

The overall integrated-growth factor e^N for each vortex between its origin and turbulent breakdown can be obtained directly from Fig. 7. The region in which turbulence was noted corresponds to vortices 4-12. The maximum-growth factor in that region was approximately e^{10}. A more precise value cannot be determined from current data because of the uncertainty in the amplitude of the initial disturbance.

Fluctuation Measurements for Disk with Single Roughness Element

Since the primary vortices for the clean disk apparently originated at microscopic disturbance sites, presumably attached dust motes, a more controlled experiment was conducted with a single, three-dimensional roughness element at a subcritical Reynolds number location. The element was 0.13 mm high ($\zeta=0.32$) by 0.64 mm square and was located at $r=100$ mm ($R=249$), $\theta=173$ deg.

The data are presented in Figs. 12-19 following the format used in presentation of the clean-disk results. Only areas where the clean and perturbed flows differ are discussed below.

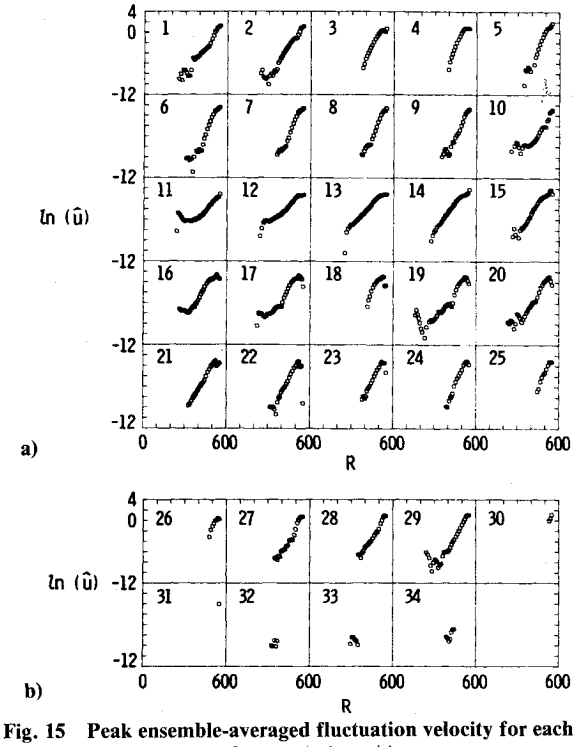

Fig. 15 Peak ensemble-averaged fluctuation velocity for each vortex on disk with roughness element (u in m/s).

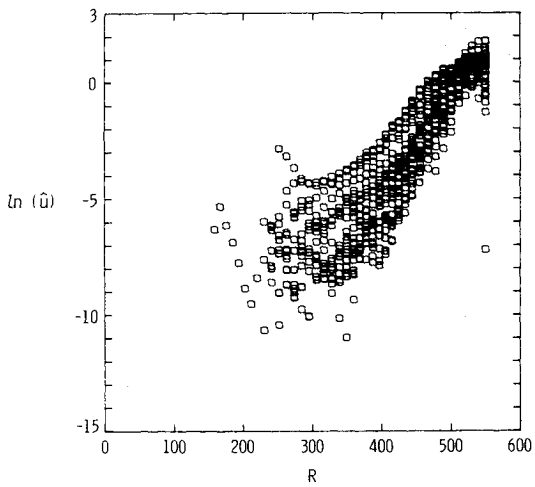

Fig. 16 Overlay of all growth data for disk with roughness element (u in m/s).

The overall, ensemble-averaged phase plot is shown in Fig. 12. The large, well-defined wave packet in the center of the plot is attributed to the roughness element. This result, along with Fig. 3, clearly suggests that the wave packets in the clean-disk flowfield originated at minute roughness elements. The vortex axes are shown in Fig. 13.

The number of vortices on the disk with the roughness element is shown in Fig. 14. The significant difference between these data and the clean-disk data (Fig. 6) is that the vortices do not become completely established (i.e., fill the entire circumference) until $R\simeq 400$ as compared to $R\simeq 350$ for the clean disk. This is apparently attributable to the fact that fewer wave packets (2 or 3) are formed on the disk with the roughness element than on the clean disk (4 or 5).

Figure 15 shows the amplitude-growth data for the vortices from Fig. 13. The most intense vortex stemming from the

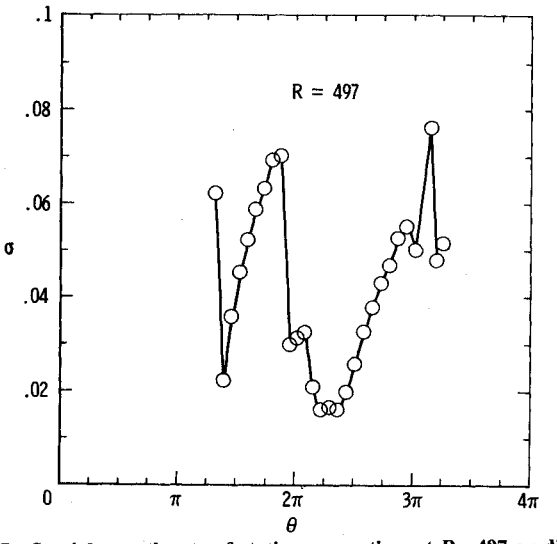

Fig. 17 Spatial growth rate of stationary vortices at $R = 487$ on disk with roughness element.

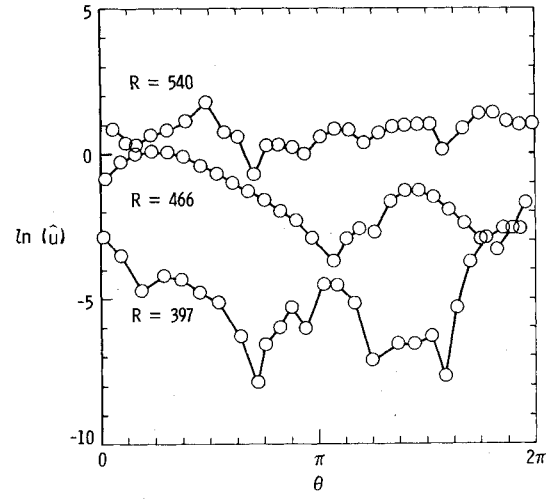

Fig. 18 Peak ensemble-averaged fluctuation velocity at three Reynolds numbers on disk with roughness element (u in m/s).

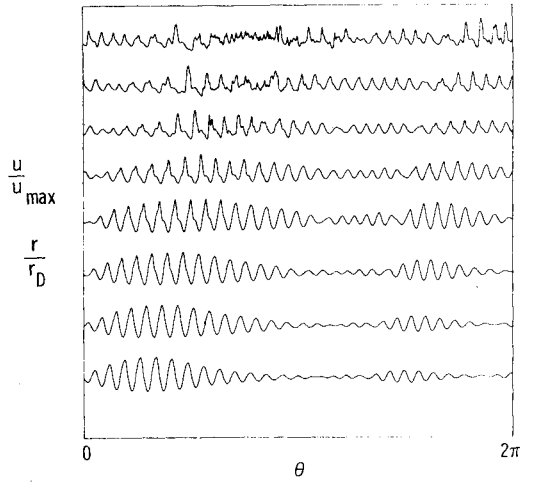

Fig. 19 Phase plot of instantaneous u in region of turbulent breakdown on a disk with roughness element. (From bottom to top: $r/r_D = 0.833, 0.852, 0.871, 0.891, 0.908, 0.924, 0.940, 0.957$.)

location of the roughness element was vortex 11. The first point on the growth plot of vortex 11 is probably not part of the organized vortex structure. The data for vortex 11 reach a minimum at $R = 339$. Data for other vortices also show a minimum above a Reynolds number of about 300 (e.g., vortices 16 and 17). The data show that vortex 19 may be two (or perhaps even three) distinct vortices as evidenced by the abrupt discontinuities in the data.

Figure 16 shows an overlay of all of the data contained in Fig. 15. Note the considerably larger circumferential variation in $\hat{u}$ than in Fig. 8. This results from the high initial disturbance amplitude of the roughness element.

Figure 17 shows the variation in the spatial growth rate with θ at a Reynolds number of $R = 497$. As in the case of the clean disk (Fig. 10), the variation in σ through a wave packet is quite large. The two smoothly varying segments in Fig. 17 correspond to the two most evident wave packets in Fig. 12. In Fig. 18, the fluctuation-velocity variation with θ is shown for three Reynolds numbers. The curve for $R = 466$ clearly shows the large-amplitude variation through the two wave packets mentioned previously. The curve for $R = 540$ illustrates the leveling off in amplitude as turbulent breakdown is approached.

Turbulent breakdown is shown in Fig. 19. Breakdown was first noted at $r/r_D = 0.924$ in the range $\pi/2 < \theta < \pi$ which corresponds to vortices 16-23. This places the transition Reynolds number in the range $521 < R_T < 530$ which is about 4% lower than the clean-disk range. As in the case of the clean disk, the overall maximum integrated-growth factor for this region was in the range of e^9 to e^{10}.

Concluding Remarks

An experimental study of the transitional flow on a flat disk rotating in quiescent ambient air has been conducted. Using digitized hot-wire data, the axes of the stationary spiral vortices, which are the primary instability mechanisms for the disk flow, have been mapped out in terms of both spatial coordinates and velocity fluctuations. Data are presented for a clean disk and a disk with a single, isolated roughness element.

Based on these data, the following conclusions can be made:

1) The stationary-vortex flowfield observed on the disk prior to transition originates at discrete, isolated disturbance sites. The sites were apparently randomly situated atmospheric-dust motes.

2) The disturbance generated by a single, three-dimensional surface roughness evolves spatially as a wave packet. The wave packets spread rapidly around the disk, merge with each other, and eventually fill the entire circumference of the disk. The modulated hot-wire oscillations, observed in the current and prior investigations of the flat disk, result from the wave-packet nature of the flowfield.

3) Stationary, secondary instabilities between the primary vortices were observed. These secondary instabilities were invariably the final stage of the transition process prior to turbulent breakdown.

4) The integrated-growth factor (measured from initiation of the disturbance to turbulent breakdown) for the wave packet resulting from dust motes was in the range e^9 to e^{10}.

5) The transition Reynolds number based on hot-wire evidence of turbulent breakdown was in the range $543 < R_T < 556$ for the clean disk and $521 < R_T < 530$ for the disk with a single, three-dimensional roughness element.

Acknowledgments

The authors would like to express their great appreciation to Dennis M. Bushnell and Mark V. Morkovin for their helpful suggestions regarding the conduct and analysis of this experiment. The work of the second author was supported under Contract NAS1-16916.

References

[1]Morkovin, M.V., "Critical Evaluation of Transition from Laminar to Turbulent Shear Layers with Emphasis on Hypersonically Traveling Bodies," AFFDL-TR-68-149, March 1969.

[2]Srokowski, A.J. and Orszag, S.A., "Mass Flow Requirements for LFC Wing Design," AIAA Paper 77-1222, Seattle, Wash., Aug. 1977.

[3]Smith, N.H., "Exploratory Investigation of Laminar Boundary Layer Oscillations on a Rotating Disk," NACA TN-1227, Dec. 1946.

[4]Gregory, N., Stuart, J.T., and Walker, W.S., "On the Stability of Three-Dimensional Boundary Layers with Application to the Flow Due to a Rotating Disk," *Philosophical Transactions of the Royal Society, London,* Ser. A, Vol. 248, 1955, pp. 155-199.

[5]Chin, D. and Litt, M., "An Electrochemical Study of Flow Instability on a Rotating Disk," *Journal of Fluid Mechanics,* Vol. 54, 1972, pp. 613-625.

[6]Kitamura, O., "Experimental Investigation on Transition of the Boundary Layer Formed on a Rotating Disk" (in Japanese), M.S. Thesis, Dept. of Mechanical Engineering, Hokkaido University, Sapparo, Japan, 1973.

[7]Fedorov, B.I., Plavnik, G.Z., Prokhorov, I.V., and Zhuknovitskii, L.G., "Transitional Flow Conditions on a Rotating Disk," *Journal of Engineering Physics,* Vol. 31, Dec. 1976, pp. 1448-1453.

[8]Kobayashi, R., Kohama, Y., and Takamadate, Ch., "Spiral Vortices in Boundary Layer Transition Regime on a Rotating Disk," *Acta Mechanica,* Vol. 35, 1980, pp. 71-82.

[9]Clarkson, M.H., Chin, S.C., and Shacter, P., "Flow Visualization of Inflectional Instabilities on a Rotating Disk," AIAA Paper 80-0279, Pasadena, Calif., Jan. 1980.

[10]Malik, M.R., Wilkinson, S.P., and Orszag, S.A., "Instability and Transition in Rotating Disk Flow," *AIAA Journal,* Vol. 19, Sept., 1981, pp. 1131-1138.

[11]Wilkinson, S.P. and Malik, M.R., "Stability Experiments in Rotating Disk Flow," AIAA Paper 83-1760, Danvers, Mass., July 1983.